Fragment mass distribution of metal cased explosive charges

W. Arnold, E. Rottenkolber

Title: Fragment mass distribution of metal cased explosive charges

Authors: W. Arnold, E. Rottenkolber

PII: S0734-743X(08)00169-3
DOI: 10.1016/j.ijimpeng.2008.07.049
Reference: IE 1651

To appear in: *International Journal of Impact Engineering*

Received Date:
Revised Date:
Accepted Date:

Please cite this article as: Arnold W, Rottenkolber E. Fragment mass distribution of metal cased explosive charges, International Journal of Impact Engineering (2008), doi: 10.1016/j.ijimpeng.2008.07.049

Fragment mass distribution of metal cased explosive charges

W. Arnold[*], E. Rottenkolber[**]
[*]*MBDA-TDW Gesellschaft für verteidigungstechnische Wirksysteme mbH, Hagenauer Forst 27, D-86529 Schrobenhausen, Germany*
[**]*NUMERICS GmbH, Mozartring 6, D-85238 Petershausen, Germany*

Abstract

Fragmentation of metal casings is an important issue in a variety of problems like weapon effectiveness, safety distances or collateral damage. To be able to describe the intended or unintended effects of naturally fragmenting shells, one needs to know the mass distribution of the fragments produced after detonation of the explosive charge. In the present study the fragmentation behavior of very light and heavier casings has been investigated. The data collection method is outlined and applied to the fragment mass distribution of four different shells. The results are given in diagrams. It was found that an existing fragmentation model adequately predicts the dependence of circumferential fragment size on material strength. Fracture in axial direction should also be considered to predict correct fragment masses, but currently a suitable model for this purpose is not available.

Keywords: Fragmentation, Metal casing, Explosive charge

1. Introduction

Effects of naturally fragmenting shells are of interest under various circumstances like predicting a weapon's effectiveness or its ability to inflict collateral damage. The effects of fragments may be unintended when shaped charges or blast charges are used to defeat a target. However, for structural reasons these charges are generally equipped with thin metal casings. On the other hand heavier steel casings are used for ammunition when the fragments are the intentional effective defeat mechanism.

In the present study the fragmentation behavior of different metal casings has been studied. Light casings were made from thin Aluminum-alloy and mild steel shells. Heavier casings were made from mild steel and hard steel. The mild steel is typical for structural applications. The hard steel was tested in two conditions, namely in the annealed condition as received from the supplier and in a heat treated condition.

The data collection method is based on image processing of photographs of witness plates, where the holes pierced by impacting fragments are detected with the help of a computer program. A variant

[*] Corresponding author. Tel.: +49 8252 996267; fax: +49 8252 996733.
E-mail address: werner.arnold@mbda-systems.com

of this method had been developed for the study of behind armor debris (BAD) clouds of steel targets caused by shaped charge jet attacks [1 to 3]. The approach used for natural fragmentation is sketched in the presented paper. The idea is to measure the hole distribution and from that to infer the mass distribution of the fragments knowing their velocity and thickness. Clearly, a couple of additional assumptions are needed to solve this problem.

The obtained mass distributions are presented within diagrams and the three different kinds of steel casings are compared. The high fragment masses produced by the hard steel casing in the annealed condition seemed to contradict not only common experience but also an existing model of circumferential fragmentation. Therefore, a closer examination is presented that finally supports the model, but also shows the need for a more general model, i.e. a model which is not restricted to circumferential fracture.

2. Experimental Study

Cylindrical explosive charges having a diameter of 100 mm and a height of 200 mm have been used for the test samples. The plastic bonded cast-cured charges were made from KS33 (= HMX/HTPB 90/10). This explosive has a density of 1.71 g/cm³ and a detonation velocity of 8480 m/s. A Gurney velocity of 2700 m/s was used to estimate fragment velocities.

Two half shells were attached to each charge. For the first trial the half shells were made from 2 mm thick aluminum alloy and mild steel. The second and third trials were done with 6 mm mild steel and hard steel casings. Properties and designations of the materials are given in Table 1.

Table 1. Casing material parameters as defined in datasheets

Casing	*Hardness HV20*	*Ultimate Tensile Strength [MPa]*	*Density [g/cm³]*	*German Designation*
2 mm, Al-Alloy	111*	370	2.85	AlCuMgPb, 3.1645.51, F37
2 mm, Mild Steel	100-150	380-450	7.86	St 35, 1.0308
6 mm, Mild Steel	100-150	380-450	7.86	St 35, 1.0308
6 mm, Hard Steel, as received	229*	750	7.85	56NiCrMoV7, 1.2714
6 mm, Hard Steel, heat treated	484* (HV50)	1550	7.85	56NiCrMoV7, 1.2714

*measured

The test set-up is shown in Fig. 1. The charges have been point-initiated with a booster (diameter 14 mm x 15 mm) from the top. The fragments from each half shell have been recorded on three witness plates made from mild steel and having a thickness of 0.5 mm. In order to avoid excessive deformation of the witness plates they were backed by low-density foam and heavier steel plates. Holes in the witness plate caused by backsplash of fragment material from the back plate could be easily identified and were removed from the data records.

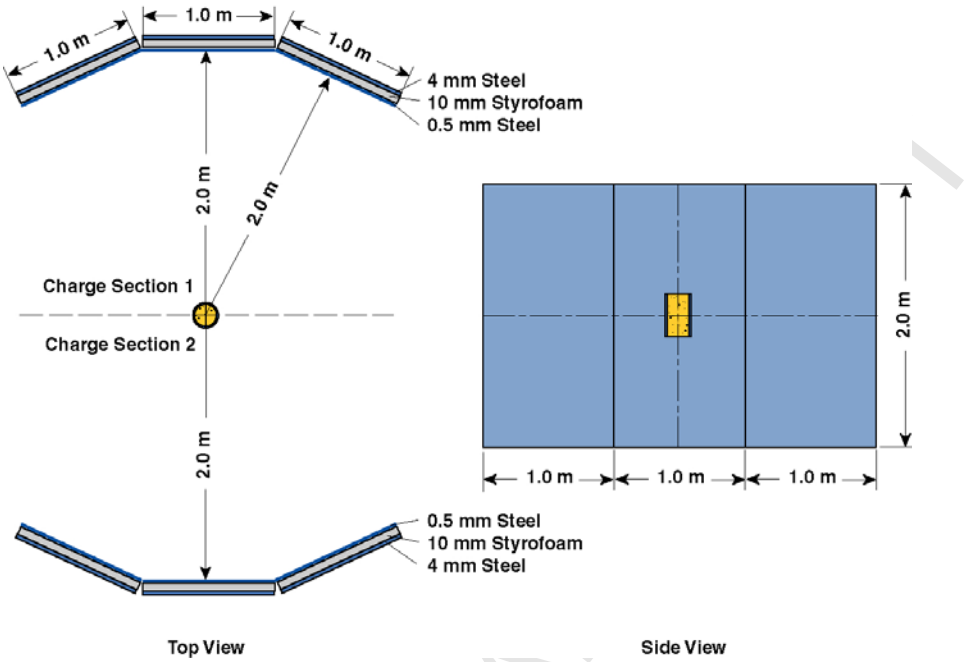

Fig. 1. Test setup with 0.5 mm steel witness plates. The charge was point-initiated from the top.

3. Data Collection Method

The applied method of data collection is based on image processing. To facilitate automatic hole detection the witness plates have to be prepared applying a definite procedure. In a first step their distortion and deformation is removed manually until an acceptably plane condition is achieved. Then the front surfaces of the plates are painted with black color and a photograph is taken with illumination from behind the plates. The effect of the preparation method is demonstrated in Fig. 2. The image obtained in this way is converted into a grayscale bitmap. Due to the high contrast of the image a simple threshold procedure is sufficient to detect the holes. Hole boundaries are stored as closed polygons and from this information the relevant data like position of the center, hole area, and orientation may be calculated. For the present purpose, namely to estimate the mass and dimensions of the fragment that pierced the hole, the hole area A_h and the length L_h and width W_h are required. Herein length and width are defined by the edges of the minimum area rectangle that contains the boundary polygon of a hole.

Determination of the fragment mass is an iterative procedure and requires some ad hoc assumptions. What we know at the outset are the initial velocity and the thickness H of a fragment. Both quantities are provided by SPLIT-X, an engineering code for the development and assessment of blast-fragmentation warheads [4]. The fragment velocity is determined by a Gurney-like method, and H is taken to be the casing thickness at breakup. The classical argument, given for example in [5], is applied to determine the state at which the casing fractures, namely when the internal pressure p equals the casing strength Y:

Fig. 2. Typical witness plate after test (left) and after preparation for evaluation (right).

$$p = Y \tag{1}$$

We take the presented area of the fragment at impact A_p as variable parameter in the iterative procedure. From the hole data we compute a form parameter λ by comparing the actual hole shape to an ellipse:

$$\lambda = \frac{A_h}{\frac{\pi}{4} W_h L_h} \tag{2}$$

Then we assume that the fragment possesses the same form factor and the same aspect as the hole, i.e. we determine the fragment width W and length L from the relations

$$\frac{L}{W} = \frac{L_h}{W_h} \tag{3}$$

$$\lambda = \frac{A_p}{\frac{\pi}{4} WL} \tag{4}$$

Since the orientation of the fragment at its impact on the witness plate is not known, we identify its actual presented area A_p with the average presented area A_c of a tumbling fragment, i.e. its so-called Cauchy-area. Then we can use the following equation to compute the volume of the fragment:

$$\frac{A_p}{V} = \frac{1}{2}\left(\frac{1}{H} + \frac{W+L}{WL}\right) \tag{5}$$

The application of this equation is justified by the fact that the equation is exact when the fragment has a rectangular shape, and that the error is less than 10% when the fragment is elliptical with L/W < 5. The iterative procedure to calculate the fragment mass is then given by the following steps:

- assume a presented area $A_{p.}$
- calculate the fragment mass with the help of equations (2) to (5).
- determine the impact velocity from the fragment mass, the presented area and the flight distance.
- compute the hole area as a function of the impact velocity, the presented area and material properties of the fragment and the witness plate.
- adjust A_p until the computed hole area matches the measured hole area.

Finally, since we know the total casing mass projected onto the witness plates, each fragment mass is scaled by an appropriate factor to force the cumulative mass to equal the expected mass. For the experiments described in the following paragraph the scaling was about 0.5 for the 6 mm casings and 0.8 for the 2 mm casings. This indicates that the shape of the fragments, especially of those produced by a thick casing, deviates considerably from that of a regular prism.

4. Experimental Results

Photographs of witness plates for every casing material and the two thicknesses are shown in Fig. 3 and 4. The calculated mass distributions are shown in Fig. 5 and 6. Fragment thickness, strain rate at fracture and initial velocity are given in Table 2. These quantities were estimated with SPLIT-X [4]. In addition, the number of perforations scaled up to a complete shell and the parameter β of a generalized Mott distribution of fragment masses can be found. The Mott distribution was determined by a least square fit and it has the following form

$$N \sim \left(1 - \exp\left(-\frac{m}{m_{ref}}\right)^{\beta}\right) \tag{6}$$

where N is the cumulative number of fragments and m is the fragment mass. The classical value $\beta = 0.5$ does not hold for the thicker steel casings. Furthermore, representing the fragmentation behavior only by the distribution function would be a poor approximation, because fragment sizes depend strongly on the axial position on the casing, which results in a non-uniform distribution on the witness plates as can be seen in Fig. 3 and Fig. 4.

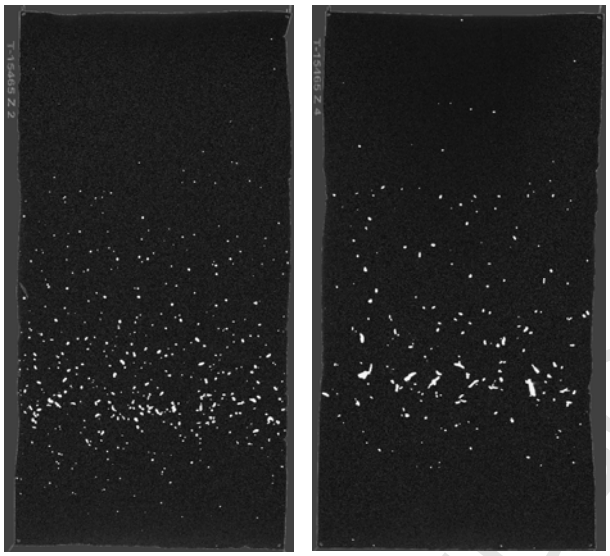

2 mm Al-Alloy 2 mm Mild Steel

Fig. 3. Sample witness plates showing hole distributions for the two 2 mm casings.

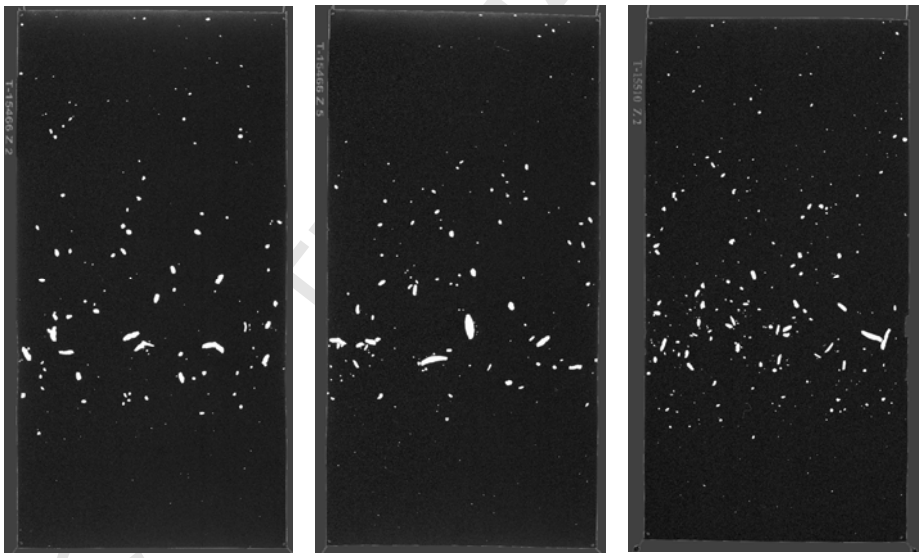

6 mm Mild Steel 6 mm Hard Steel, as received 6 mm Hard Steel, heat treated

Fig. 4. Sample plates showing hole distributions for three 6 mm casings.

Table 2. Fragment mass distribution data

Casing	*Total Number of Perforations*	*Mott Parameter β*	*Fragment Thickness H [mm]*	*Strain Rate at Fracture [1/s]*	*Initial Velocity [m/s]*
2 mm Al-Alloy	6568	0.55	1.5	$5.0 \cdot 10^4$	3217
2 mm Mild Steel	2868	0.48	1.3	$4.0 \cdot 10^4$	2667
6 mm Mild Steel	2338	0.35	3.7	$2.7 \cdot 10^4$	1819
6 mm Hard Steel, as received	2726	0.29	4.1	$2.8 \cdot 10^4$	1819
6 mm Hard Steel, heat treated	4587	0.31	4.6	$2.9 \cdot 10^4$	1819

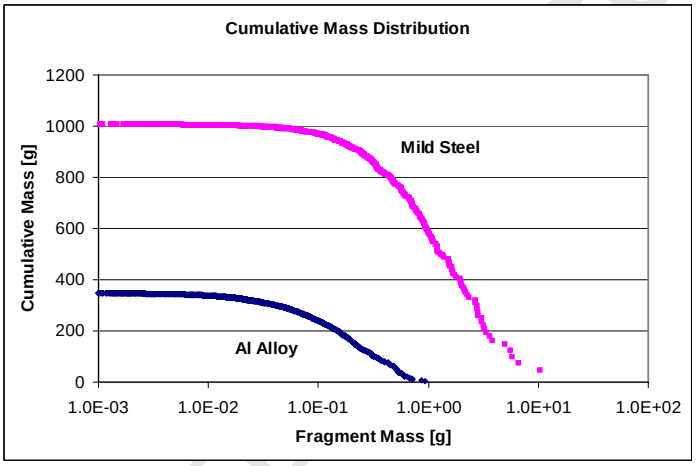

Fig. 5. Cumulative mass distributions of 2 mm Al and Steel casings.

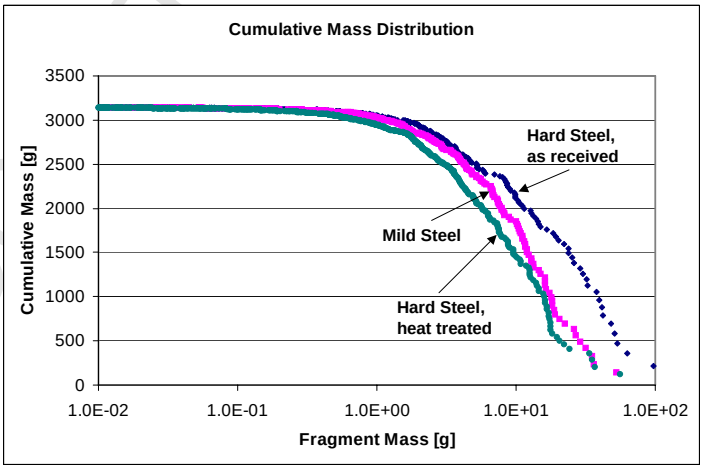

Fig. 6. Cumulative mass distributions of 6 mm steel casings.

5. Theoretical Considerations

Based on common experience it was expected that the annealed hard steel casing would produce smaller fragments when compared to the mild steel casing. Looking at Fig. 6, the opposite seems to have happened. Therefore we had to examine a known fragmentation model in more detail. The model of Grady and Hightower [5] has been developed for fragmenting steel casings of high explosive charges. Based on energy considerations the authors derived an equation for the circumferential fracture spacing, i.e. the nominal fragment width S:

$$S = \left(\frac{24\Gamma}{\rho \dot{\varepsilon}^2} \right)^{\frac{1}{3}}, \tag{7}$$

where $\dot{\varepsilon}$ is the strain rate, ρ is the mass density, and Γ is the fracture energy per unit area. The model considers two predominant modes of fracture in the breakup of an expanding metal shell, which are illustrated in Fig. 7. The first is tensile fracture where failure proceeds by crack propagation. This fracture mode is governed by the material's fracture toughness K_C, and an expression for the fracture energy is provided by

$$\Gamma_{\text{Tensile}} = \frac{K_c^2}{2E}, \tag{8}$$

where E is the elastic modulus of the material.

Shear fracture initiated by adiabatic shear banding is the second important mode of failure. According to [5] the shear fracture energy is given by the expression

$$\Gamma_{\text{Shear}} = \frac{\rho c}{\alpha} \left(\frac{9\rho^3 c^2 \chi^3}{Y^3 \alpha^2 \dot{\varepsilon}} \right)^{\frac{1}{4}}. \tag{9}$$

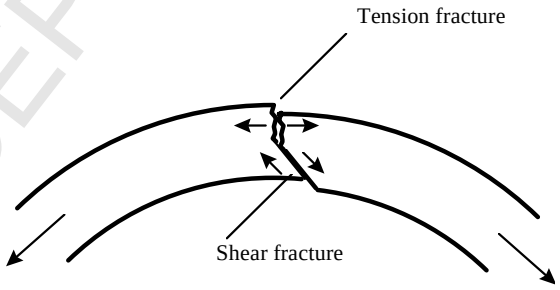

Fig. 7. Tension and shear fracture as the two basic failure modes [5].

Material properties entering this equation are the specific heat c, the thermal diffusion coefficient χ, the thermal softening coefficient α, and the plastic flow stress Y. It is empirically known that shear fracture is the dominant mode when the fracture toughness is high and the casing is not too thick. Both conditions are fulfilled for the three different 6 mm steel casings in our trials. Therefore, we can use Eqn (9) to estimate the ratio of fracture energies, and Eqn (7) to calculate the ratio of nominal fragment widths, which are shown Table 3.

Table 3. Calculated fragment widths relative to the mild steel casing

Casing	*Y [MPa]*	*Calculated Fragment Width*
6 mm Mild Steel	450	S
6 mm Hard Steel, as received	750	0.88 S
6 mm Hard Steel, heat treated	1550	0.73 S

Looking at the hole width distribution of the largest holes in Fig. 8, we indeed find slightly greater values for the mild steel in accordance with the shear fracture model. The larger fragment masses of the annealed hard steel must therefore be due to greater fragment lengths, which are confirmed by the distribution of hole lengths shown in Fig. 9. Whereas circumferential spacing, i.e. fragment width, decreases with higher material strength, this is not the case for axial spacing, where the material with the intermediate strength produces the longest fragments. The relatively low axial strain rate, especially in the central region of a detonating cylindrical shell, is probably the quantity responsible for this behavior. Consequently the shear fracture model discussed above is not applicable at low strain rates. However, to the best of our knowledge, no model is available which is adequately suited for our problem.

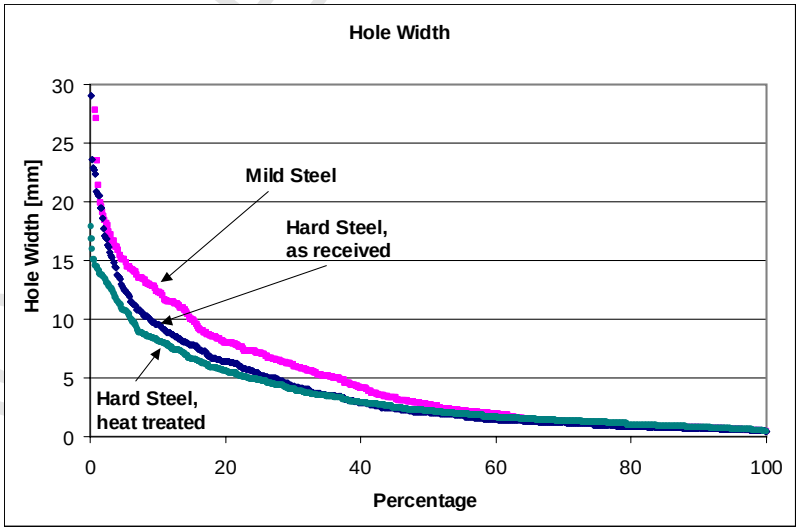

Fig. 8. Hole width of fragments from the 6mm mild and hard steel casings.

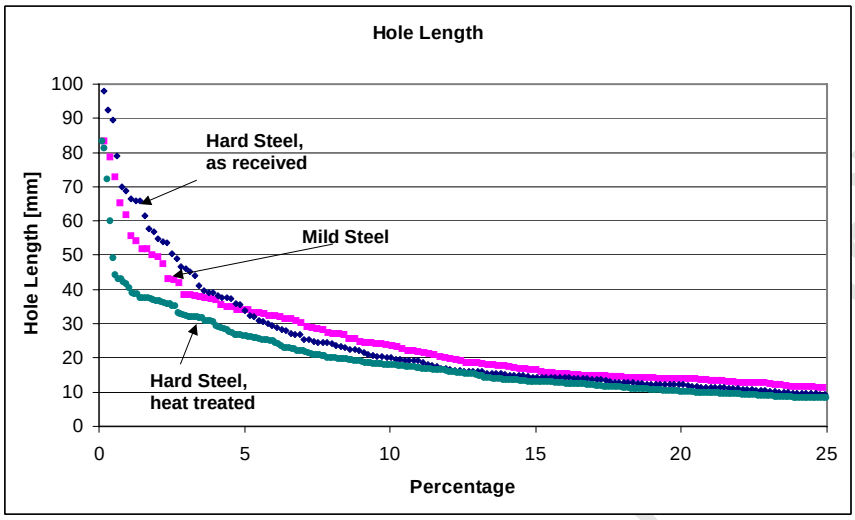

Fig. 9. Hole length of fragments from 6 mm mild and hard steel casings.

6. Conclusions

A method for fast data collection of fragmenting shells was sketched. The method was applied to generic casings of missile warheads and heavier cased ammunitions. Mass distributions gained by this method were presented for four different cases. Comparing three steel casings made of materials having different strength, we surprisingly found the largest fragments for the casing with the intermediate material strength. A closer examination revealed that fragment widths from this material were in accordance with a known fragmentation model. However in axial direction the steel casing with the intermediate strength produced the longest fragments. Development of a fragmentation model suitable for axial fracture remains a task for future activities.

References

[1] Arnold W, Paul W. Behind armor debris investigation and their application into a New Vulnerability Model. *Int. J. Impact Eng.*, 2001; **26**: 21-32.

[2] Arnold W, Rottenkolber E. Behind armor debris investigation (Part II). *Int. J. Impact Eng.*, 2003; **29**: 95-104.

[3] Arnold W, Rottenkolber E. Physics of behind armor debris threat reduction *Int. J. Impact Eng.*, 2006; **33**: 53-61.

[4] SPLIT-X, Modeling of natural fragmentation, NUMERICS GmbH, Petershausen, Germany, 2005

[5] Grady DE, Hightower MM. Natural fragmentation of exploding cylinders, *International Conference on the Materials Effects of Shock-wave and High-strain-rate phenomena*, 1990; 713-721.